



HAL
open science

Identification and Extraction of Seasonal Geodetic Signals Due to Surface Load Variations

S Laroche, A Gualandi, Kristel Chanard, Jean-philippe Avouac

► **To cite this version:**

S Laroche, A Gualandi, Kristel Chanard, Jean-philippe Avouac. Identification and Extraction of Seasonal Geodetic Signals Due to Surface Load Variations. *Journal of Geophysical Research: Solid Earth*, 2018, 123 (12), pp.11031-11047. 10.1029/2018jb016607. hal-03938718

HAL Id: hal-03938718

<https://hal.science/hal-03938718>

Submitted on 13 Jan 2023

HAL is a multi-disciplinary open access archive for the deposit and dissemination of scientific research documents, whether they are published or not. The documents may come from teaching and research institutions in France or abroad, or from public or private research centers.

L'archive ouverte pluridisciplinaire **HAL**, est destinée au dépôt et à la diffusion de documents scientifiques de niveau recherche, publiés ou non, émanant des établissements d'enseignement et de recherche français ou étrangers, des laboratoires publics ou privés.

RESEARCH ARTICLE

10.1029/2018JB016607

Key Points:

- We propose a procedure to isolate seasonal geodetic signals due to surface loads using a GRACE-based deformation model and an independent component analysis
- GNSS and GRACE-derived displacements yield consistent seasonal time evolutions in both the Arabian Peninsula and the Nepal Himalaya
- The method is robust to topographic and elastic heterogeneities, simple moving loads and geodetic products errors

Supporting Information:

- Supporting Information S1
- Movie S1

Correspondence to:

S. Larochele,
stacy.larochele@caltech.edu

Citation:

Larochele, S., Gualandi, A., Chanard, K., & Avouac, J.-P. (2018). Identification and extraction of seasonal geodetic signals due to surface load variations. *Journal of Geophysical Research: Solid Earth*, 123, 11,031–11,047. <https://doi.org/10.1029/2018JB016607>

Received 23 AUG 2018

Accepted 16 NOV 2018

Accepted article online 22 NOV 2018

Published online 15 DEC 2018

©2018. American Geophysical Union.
All Rights Reserved.

Identification and Extraction of Seasonal Geodetic Signals Due to Surface Load Variations

S. Larochele¹ , A. Gualandi^{1,2} , K. Chanard³ , and J.-P. Avouac¹ 

¹Geological and Planetary Sciences, California Institute of Technology, Pasadena, CA, USA, ²Jet Propulsion Laboratory, NASA, Pasadena, CA, USA, ³LASTIG LAREG, IGN, ENSG, Université de Paris Diderot, Sorbonne Paris Cité, Paris, France

Abstract Deformation of the Earth's surface associated with redistributions of continental water mass explains, to first order, the seasonal signals observed in geodetic position time series. Discriminating these seasonal signals from other sources of deformation in geodetic measurements is essential to isolate tectonic signals and to monitor spatio-temporal variations in continental water storage. We propose a new methodology to identify and extract these seasonal signals. The approach uses a variational Bayesian Independent Component Analysis (vbICA) to extract the seasonal signals and a gravity-based deformation model to identify which of these signals are caused by surface loading. We test the procedure on two study areas, the Arabian Peninsula and the Nepal Himalaya, and find that the technique successfully extracts the seasonal signals with one or two independent components, depending on whether the load is stationary or moving. The approach is robust to spatial heterogeneities inherent to geodetic measurements and can help extract systematic errors in geodetic products (e.g., draconitic errors). We also discuss how to handle the degree-1 deformation field present in the geodetic data set but not captured by the gravity-based model.

1. Introduction

Seasonal signals are observed in geodetic position time series of Global Navigation Satellite System (GNSS) stations at a global scale (Blewitt et al., 2001). These annual displacements can be explained, to first order, by the Earth's response to variations in surface loads mostly due to redistributions of continental water mass (Blewitt et al., 2001; Dong et al., 2002; van Dam et al., 2001). Identifying and extracting nontectonic seasonal signals from geodetic measurements is critical to detect potential tectonic signals of small amplitude, key to our understanding of the seismic cycle (e.g., slow slip events and tremors, postseismic slip, and interseismic strain). Characterizing geodetic seasonal signals is also important to study the possible relationship between small periodic stresses and earthquake nucleation (Bettinelli et al., 2008; Bollinger et al., 2007; Craig et al., 2017; Johnson et al., 2017), invert for continental water storage fluctuations (Argus et al., 2014; Borsa et al., 2014; Fu et al., 2015), and constrain the elastic (Chanard et al., 2014; Drouin et al., 2016) and viscoelastic (Chanard, Fleitout, Calais, Barbot, & Avouac, 2018) properties of the Earth.

In recent years, two promising strategies to isolate geodetic seasonal signals have been developing in parallel. On one hand, a large effort has been made toward developing accurate models of the Earth's surface displacements induced by surface load variations measured by the Gravity Recovery and Climate Experiment (GRACE) satellites (Figure 1). Several studies (Bettinelli et al., 2008; Chanard et al., 2014; Chanard, Fleitout, Calais, Rebeschung, & Avouac, 2018; Davis et al., 2004; Fu et al., 2012; Fu & Freymueller, 2012) have demonstrated that GRACE-based deformation models can explain a large part of the GNSS annual observations. Although such models are essential to establish the hydrological origin of seasonal geodetic signals, discrepancies remain between model and data (e.g., Figures 2a and 2b).

On the other hand, the task of isolating seasonal signals from geodetic time series can be approached as a blind-source separation problem where the observed displacements are the result of several, mixed sources. To this end, an independent component analysis (ICA) can be applied to the displacement data set to untangle, in a purely statistical manner, the different physical processes beneath the observations (Comon, 1994). Notably, Gualandi, Avouac, et al. (2017), Gualandi, Nichele, et al. (2017), and Serpelloni et al. (2018) showed that the variational Bayesian form of the ICA (vbICA) can objectively extract seasonal signals from GNSS time series. Being a data-driven approach, ICA-reconstructed seasonal signals have the ability to satisfactorily reproduce the observations, capturing also the effects of local heterogeneities that are otherwise

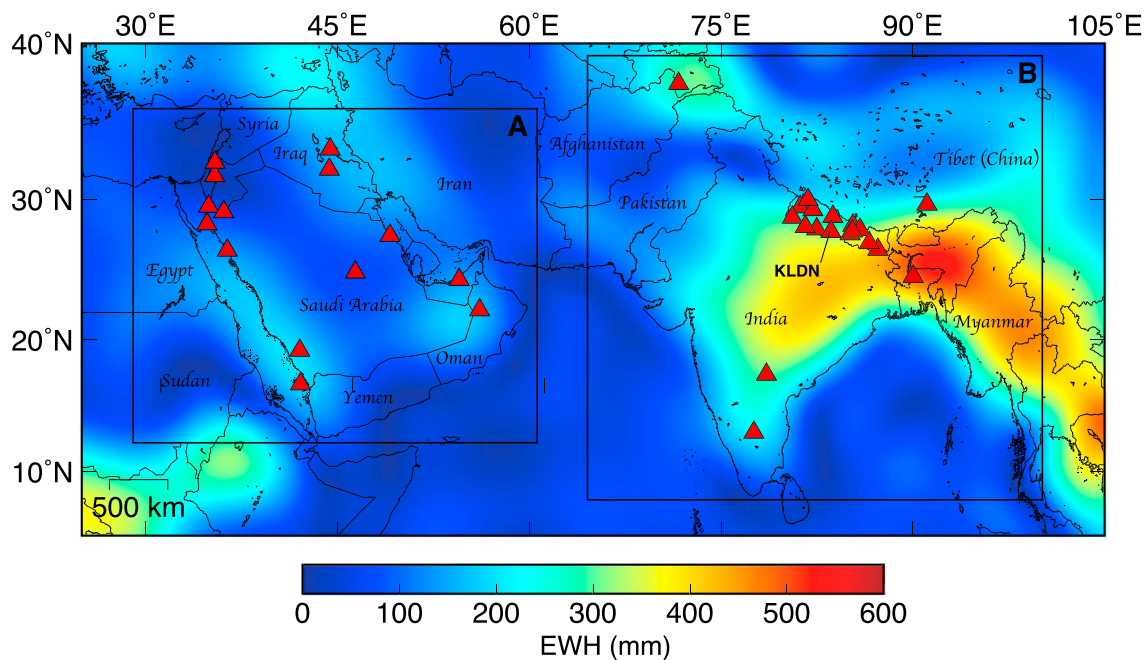


Figure 1. Average peak-to-peak GRACE-derived surface load distribution for the period 2007 to 2012.5 expressed in equivalent water height (EWH). Boxes A and B delineate the two study areas: the Arabian Peninsula and the Nepal Himalaya. The triangles indicate the locations of GNSS stations used in each study area. Station KLDN for which time series are shown in Figure 2 is also identified.

averaged out in the aforementioned models. While the independence of components required by ICA suggests that these seasonal components are physical signals, the technique alone provides no information about their origins.

In light of the strengths and limitations of these two parallel strategies, we here propose a procedure that combines the physical robustness of a GRACE-based model (Chanard et al., 2014; Chanard, Fleitout, Calais, Rebischung, & Avouac, 2018) with the statistical precision of the vbICA algorithm (Gualandi et al., 2016) to (1) decompose the displacement data sets (GNSS and GRACE-derived deformation) into a finite number of components, (2) retain the seasonal signals, and (3) describe them in terms of underlying physical processes. Hereafter, we first present the GNSS data and GRACE-derived deformation model used in this study and provide an overview of the vbICA technique and the proposed procedure. In section 3, we test the procedure in two study areas: the Arabian Peninsula and the Nepal Himalaya. Each case study presents its own complexities and provides complementary insight on the robustness of the approach to spatial heterogeneities and how it can help extract systematic errors in geodetic products (e.g., draconitic errors). In section 4 we explore two variations to the input time series in order to identify the most robust procedure, which we summarize in section 5. We conclude with final remarks on the applicability of the procedure.

2. Data and Methods

2.1. Data Sets

2.1.1. GNSS Displacement Time Series

We use 24-hr final solution time series processed by the Nevada Geodetic Laboratory (NGL; Blewitt et al., 2018). The solutions are aligned with ITRF2008 whose origin linearly tracks the mean of the total Earth system's center of mass but corresponds to the center of the IGS08b network, which is close to the center of figure of the Earth for subsecular time scales (Dong et al., 2003). Most of the available continuous GNSS stations in the regions of interest were deployed in 2007 or later. To minimize missing data across the GNSS and GRACE data sets, we consider the time range (2007.0, 2012.5) since the GRACE data started showing more frequent gaps in 2012 as the satellites neared the end of their lifespan (Jean et al., 2015). Of the 72 GNSS stations available in the Arabian Peninsula and of the 59 available in Nepal, for each area we select 14 stations with recordings during the time range (2007.0, 2012.5) in such a way that the stations are approximately evenly distributed across the studied region. Five stations outside of Nepal are also included to ensure that

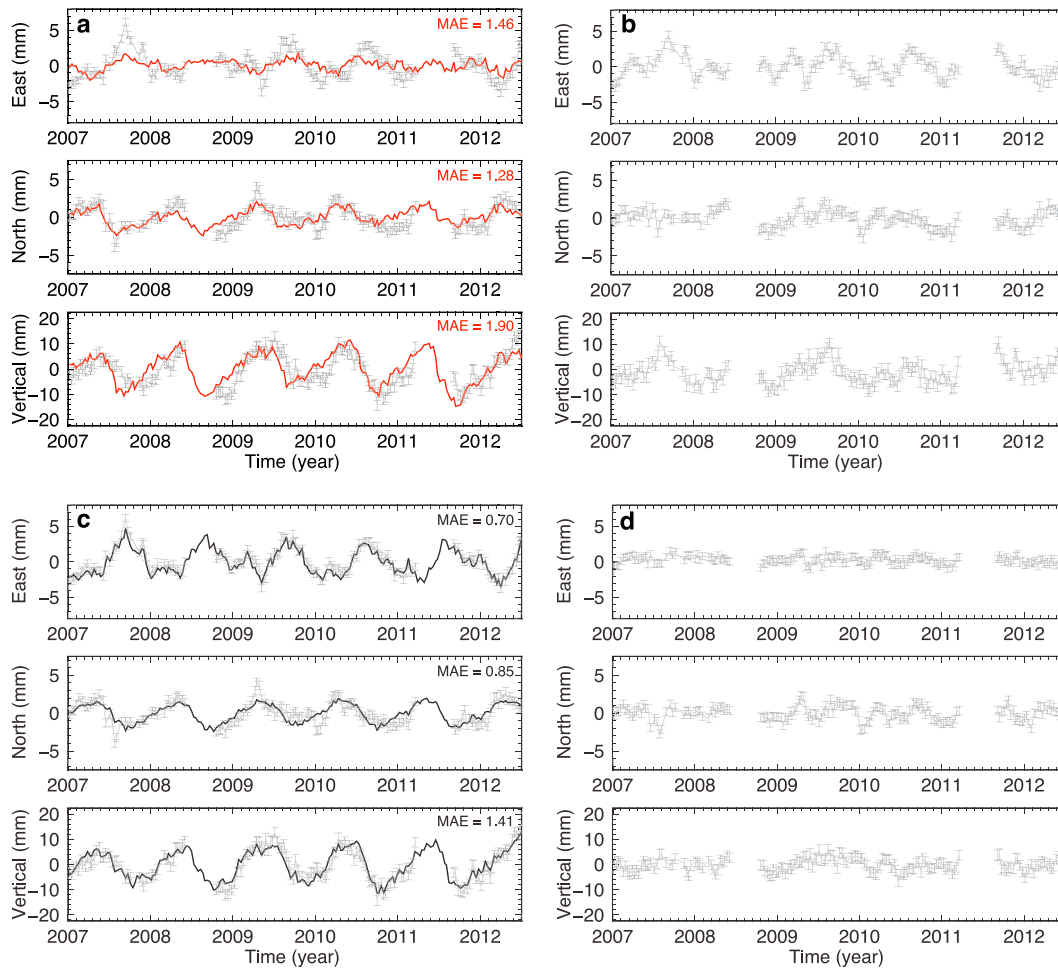


Figure 2. Comparison of seasonal correction at GNSS station KLDN in Nepal from the GRACE model and the recommended variational Bayesian Independent Component Analysis (vbICA) reconstruction with two ICs. (a) East, north, and vertical components of the detrended 10-day moving-average geodetic (grey) and GRACE model (red) data sets with the mean absolute error indicated at the top right corner. (b) GNSS time series corrected for seasonal signal (via subtraction of GRACE model). (c and d) Same as (a) and (b) but for the vbICA reconstruction (black) proposed in this study. As indicated by the MAE values and the residuals in (b) and (d), the vbICA reconstruction performs better at removing the seasonal signals in the original GNSS time series.

loads with a spatial wavelength larger than Nepal are fully captured. The selected stations are indicated by triangles in Figure 1.

The geodetic time series are simultaneously detrended and corrected for step discontinuities by least squares fitting of a linear trend, annual and semiannual sinusoids, and offsets terms where visually obvious (see Table S1), at epochs corresponding to equipment changes, and coseismic displacements as reported by NGL (<http://geodesy.unr.edu/NGLStationPages/steps.txt>). Note that detrending is necessary when comparing GNSS and GRACE-derived data sets as they may not exhibit the same long-term trends (e.g., interseismic deformation might be present in the GNSS data set but not in GRACE). This means that, here, we are only comparing the variations from the relative linear trends of the two data sets. Note, however, that the technique does not require the linear trend in the GNSS time series to be of tectonic origin only. Outliers, defined as data points that exceed 3 times the average deviation from the mean within a 90-day sliding window in any of the directions (east, north, and vertical), are then removed from all three time series relative to a given station. The daily position solutions are also averaged over a 10-day period to match the GRACE data temporal resolution.

The final step consists in removing the spherical harmonics degree-1 contribution from the time series to allow comparison with the GRACE data set, which does not contain degree-1 deformations (Swenson

et al., 2008). We estimate and retrieve the degree-1 deformation field using a data set of 689 globally distributed GNSS time series processed by NGL (Blewitt et al., 2018), as described in Chanard, Fleitout, Calais, Rebischung, and Avouac (2018). The importance of the degree-1 deformation field and the necessity of correcting for its effect in the GNSS time series are discussed in further details in section 4.1. These final time series are referred to as the GNSS data set. Figure 2 shows an example of cleaned GNSS time series at station KLDN in Nepal. Additional time series at other stations are also available in Figure S1.

2.1.2. GRACE Gravimetric Time Series

To quantify surface mass variations, we start with the 10-day Level-2 CNES/CRGS solutions (<http://grgs.obs-mip.fr>, last accessed on 1 July 2017) of the Earth's time-varying gravitational field as measured by the GRACE twin satellites. The CNES/CRGS processing methodology, which includes removal of the static geoid and of well-characterized gravimetric contributions (e.g., solid Earth and oceanic tides), is described in Bruinsma et al. (2010). We add back atmospheric and nontidal oceanic contributions as these are not corrected for in the GNSS data set (Carrère & Lyard, 2003). The solutions expressed in terms of Stokes coefficients of degree 2 to 50 are converted, via isotropic filtering (Ramillien et al., 2005), to a spatial load distribution in units of equivalent water height (EWH). The EWH time series are then detrended to allow comparison with the geodetic data set. Figure 1 shows the resulting peak-to-peak surface load distribution averaged over the study period of 2007 to 2012.5.

2.1.3. GRACE-Derived Displacement Time Series

To enable comparison between the GRACE and GNSS data sets, we compute the displacements expected at the GNSS site locations from the GRACE-derived surface load distribution by using the numerical model developed by Chanard, Fleitout, Calais, Rebischung, and Avouac (2018). The model first decomposes the loads in the temporal and spatial domains and generates load Love numbers (Farrell, 1972) for an elastic Earth structure with continental crust (Bassin et al., 2000) and preliminary reference Earth model parameters (Dziewonski & Anderson, 1981). The spatially and temporally separated loads are then convolved with the appropriate load Love numbers to form the desired displacement time series. Figure 2a shows an example of a GRACE-derived time series at station KLDN. Hereafter, we refer to this data set as the GRACE data set.

2.2. Variational Bayesian Independent Component Analysis (vbICA)

The goal of any ICA algorithm is to isolate a set of ICs that when mixed together can explain the observations. As is usual of ICA algorithms (e.g., JADE, Cardoso & Souloumiac, 1993; or FastICA, Hyvärinen & Oja, 1997), the vbICA framework is set up as a linear mixing problem of nonmoving sources, that is,

$$X = A\Sigma + N \quad (1)$$

where X is the matrix of the input time series, A is the mixing matrix, Σ is the sources matrix, and N is Gaussian noise. The mixing matrix A only depends on the relative position between the stations and the sources, while matrix Σ contains the temporal functions characterizing the sources. Differently from conventional ICA algorithms, however, vbICA follows a modeling approach; that is, it searches for some best (in a sense to be defined) model parameters. This offers two advantages: (1) Data gaps can be handled without any interpolation of the missing data (Chan et al., 2003; Gualandi et al., 2016) and (2) we gain flexibility in the description of the sources. In particular, the sources are modeled by a mixture of Gaussians (MoG). Since any probability density function (pdf) can be expressed as a MoG, given a sufficient number of Gaussians, the technique is capable of generating multimodal pdfs commonly observed in geophysical signals (Gualandi et al., 2016).

Under the Bayesian framework, the modeling approach attempts to maximize the posterior pdf of the model parameters, that in our case are random variables related to the mixing matrix, the noise and the sources. We refer to Gualandi et al. (2016) for a list of all the parameters W involved in the model. The best model parameter set is that which simultaneously maximizes the statistical independence of the sources' pdfs and the fit to the data. Maximizing the parameters' posterior pdf is a challenging task that vbICA accomplishes by using a variational approximation approach which consists in introducing an approximating pdf ($p'(W)$) to the real posterior pdf ($p(W|X)$). The best approximation is the one that minimizes the Kullback-Leibler (KL) divergence between $p'(W)$ and $p(W|X)$, defined as

$$D_{KL}[p'(W) \| p(W|X)] = \int p'(W) \ln \left[\frac{p'(W)}{p(W|X)} \right] dW \quad (2.1)$$

Since the true posterior pdf is unknown, we resort to variational inference and Bayes theorem to rewrite equation (2.1) as

$$\begin{aligned} D_{KL}[p'(W) \| p(W|X)] &= -\int p'(W) \ln \left[\frac{p'(W)}{p(W, X)} \right] dW + \int p'(W) \ln[p(X)] dW \\ &= -\int p'(W) \ln \left[\frac{p'(W)}{p(W, X)} \right] dW + \ln[p(X)] \end{aligned} \quad (2.2)$$

Since the log-evidence $\ln[p(X)]$ does not depend on W , we can maximize the integral term (called the Negative Free Energy) with respect to $p'(W)$ in order to minimize the KL divergence on the left-hand side of (2.2).

The Bayesian framework also requires that a priori parameters (or hyperparameters) be specified for the pdfs governing the model parameters W . In practice, the choice of priors affects how much the model is allowed to adapt to the observations. However, since the GNSS data set under study here is not particularly affected by the choice of prior on the mixing matrix and sources, we select a priori hyperparameters that let the data dominate the a posteriori pdf. For the GRACE data set, we use the same priors on the mixing matrix and sources precision but select modified values for the noise precision to account for the increased signal-to-noise ratio (SNR) inherent to modeled data sets. These sets of hyperparameter values are specified in Table S2 of the supporting information. A brief description of these hyperparameters is also presented in the footnote of Table S2.

We aggregate the time series from the two data sets into matrices $X_{M \times T}$ where M is the number of time series (equal to 3 times the number of stations to account for the east, north, and vertical directions) and T the number of epochs. We follow the notation of Gualandi et al. (2016), where similarly to a singular value decomposition notation, the data set is decomposed into three matrices:

$$X_{M \times T} \sim U_{M \times R} S_{R \times R} V_{R \times T}^T \quad (3)$$

where R is the number of components, $U_{M \times R}$ is the matrix of spatial distributions, $S_{R \times R}$ is a weighting diagonal matrix, and $V_{R \times T}$ is the matrix of temporal functions. The only difference between the notation of equations (1) and (3) is the introduction of the diagonal matrix S , which is obtained after setting the columns of U and V to unit norm. Contrary to singular value decomposition and the commonly used principal component analysis, the columns of U and V are not orthogonal and the weights in S do not directly relate to the variance of the data set. Hereafter, we refer to the spatial distribution, weight, and temporal function of the i th component as U_i , S_i , and V_i , respectively, with $i = 1, \dots, R$.

To decide on the number of components to retain, we resort to the Automatic Relevance Determination (ARD) criterion posed in Gualandi et al. (2016). The ARD criterion relies on the variances of the mixing matrix columns, which can be computed from the derived mixing matrix posterior pdf. If the posterior variance of one column is small (<10 times) compared to the variance of the other columns, this implies that the corresponding IC contributes very little to the data reconstruction as its mixing values remain close to the null a priori. We thus select the number of components to be one less than the number of ICs at which one IC becomes unimportant for the data reconstruction.

2.3. Proposed Procedure

The procedure we propose to extract geodetic seasonal signals aims to identify components that share the same physical mechanism in the GNSS and GRACE-derived data sets. The step-by-step procedure can be summarized as follows:

1. Generate GRACE-derived displacement time series using the model presented in Chanard, Fleitout, Calais, Rebischung, and Avouac (2018).

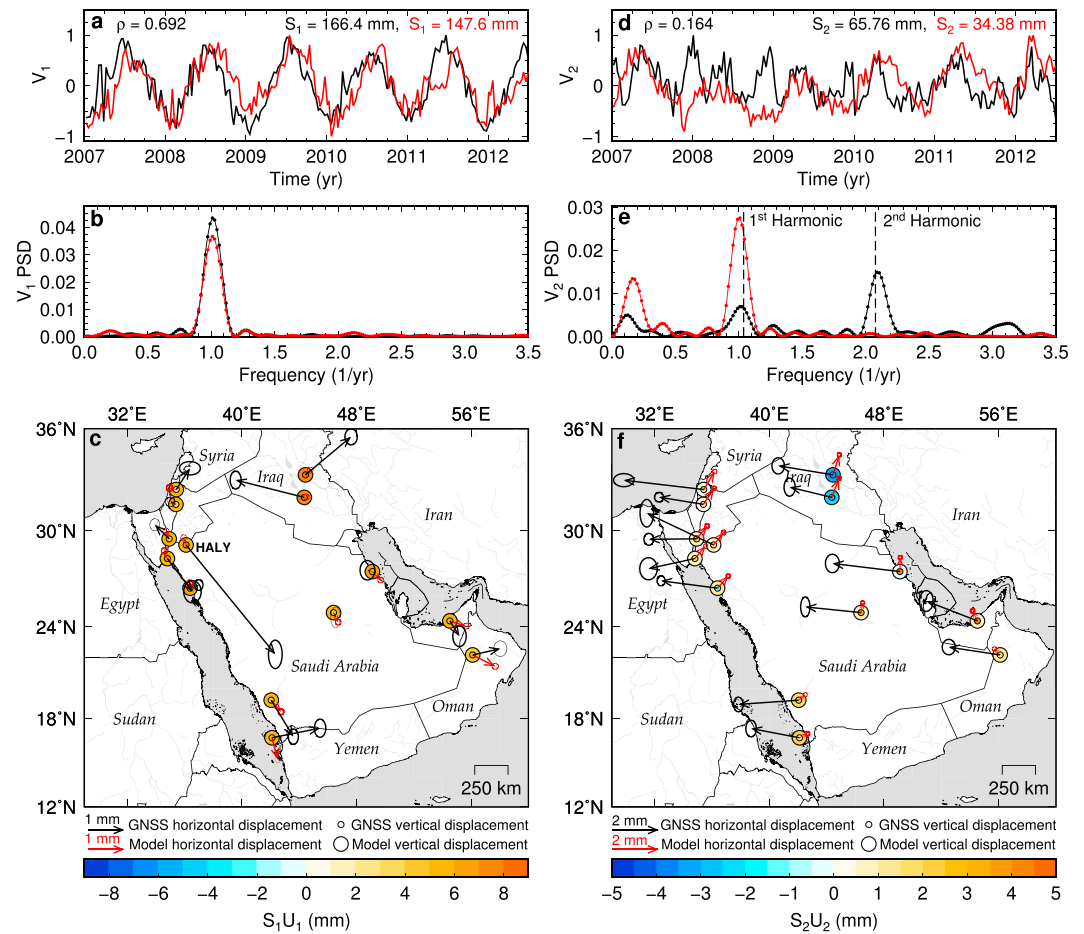


Figure 3. vbICA results for the Arabian Peninsula case for degrees >1 . (a and d) Temporal functions (V) for IC_1 and IC_2 from the GNSS data set (black) and the GRACE model (red). The correlation coefficients and S values are reported in each case in the top left and right corners, respectively. (b and e) Power spectral densities associated with the temporal functions in (a) and (d). The first and second draconitic harmonics are indicated by dashed lines. (c and f) Spatial distribution (U) of IC_1 and IC_2 . The arrows are the horizontal displacement for the GNSS data (black) and the GRACE model (red). The uncertainty ellipses for the spatial distributions correspond to 1σ confidence intervals. The circles are the vertical displacement for the GNSS data (inner circle) and the GRACE model (outer circle). U has been multiplied by the appropriate S in order to express the spatial distribution in mm. While IC_1^{GNSS} and IC_1^{GRACE} are seasonal and matching, IC_2^{GNSS} and IC_2^{GRACE} are not. IC_2^{GNSS} is instead attributed to draconitic effects.

2. Perform vbICA with an increasing number of ICs on the GNSS data set until the ARD criterion is satisfied.
3. Perform vbICA on the GRACE data set with the number of ICs identified in step 2).
4. (a) Starting with the GNSS IC with the highest weight S_i , compare the temporal function V_i with the remaining unmatched GRACE temporal functions by computing correlation coefficients (ρ).
(b) Pair GNSS IC_i with the GRACE IC with which it has the highest ρ .
(c) If the correlation is higher than 0.50, consider the match a good one.

Tables S3 and S4 demonstrate how this pairing process is done in the Arabian Peninsula and the Nepal Himalaya, respectively.

5. Reconstruct the geodetic seasonal signal from the GNSS ICs having a good match with GRACE ICs.

Note that the above procedure is only meant as a general guideline for potential users of this technique and can be modified as needed. The 0.50 correlation coefficient criterion, for example, is somewhat arbitrary and could be modified, as long as there is some methodology in place to match the ICs across the two data sets.

Table 1
Correlation Coefficients Between the GNSS-GRACE Model IC Pairs Shown in Figures 3, 5, and 7–10

Decomposition direction	Degrees >1		All degrees	
	IC ₁	IC ₂	IC ₁	IC ₂
Arabian Peninsula				
Combined	0.692	0.164	0.747	0.115
Horizontal	−0.012	−0.030	0.523	0.208
Vertical	0.623	0.039	0.581	−0.013
Nepal Himalaya				
Combined	0.823	0.628	0.843	0.528
Horizontal	0.837	0.667	0.699	0.019
Vertical	0.841	0.745	0.847	0.747

Note. The combined approach with degrees > 1 refers to the original analysis performed in section 3. The all-degrees and horizontal/vertical analyses are presented in sections 4.1 and 4.2, respectively.

3. Case Studies

3.1. Arabian Peninsula

As a first test case, we apply the proposed technique to the Arabian Peninsula—a region with a relatively simple but important seasonal loading pattern (e.g., Figures S1v–S1viii). The first two ICs (shown in Figure 3) explain about 55% of the data variance in the GNSS data set and are found to be sufficient to satisfy step 2) of the procedure. Looking at the temporal functions of the ICs, we find that V_1^{GNSS} and V_1^{GRACE} are both seasonal and agree well with one another ($\rho = 0.692$; Table 1 and Figure 3a), providing strong evidence to conclude that the seasonal signal in Arabia is of hydrological origin. Although establishing the exact hydrological cause(s) of the signal is outside the scope of this study, we expect the hydrological seasonality to be at least partially caused by the inflow of water in the Red Sea (from the Gulf of Aden) in the fall and the subsequent outflow in the spring, both resulting from the Monsoon climate (Smeed, 2004; Wahr et al., 2014).

As for the spatial distributions U_1^{GNSS} and U_1^{GRACE} , there is good agreement in the vertical direction, but discrepancies are visible in the horizontal directions. We see two potential reasons for these discrepancies: (1) The GRACE data set is derived from long-wavelength gravity measurements (>200 km), whereas GNSS observations are local measurements. Geodetic measurements can thus be affected by local heterogeneities (e.g., in mass, Earth rheology, or in surface load due to basins and rivers) that are averaged out in the GRACE data set. This is especially true for horizontal GNSS measurements, which are more sensitive to small-wavelength heterogeneities than vertical measurements. For example, the large-amplitude observed at GNSS station HALY (Figure 3c) could be due to a nearby body of groundwater with high seasonality. (2) The signal extracted from the GNSS data set is still mixed with other physical effects (e.g., poroelastic and thermoelastic) or potential systematic GNSS processing errors both not captured by gravimetric measurements. In other words, there might be cross-talk (i.e., leakage of one IC into another) between the ICs. Given the high correlation between V_1^{GNSS} and V_1^{GRACE} , we argue that cross-talk is negligible in this case.

To investigate the first possibility, in Figure 4, we demonstrate how a heterogeneous load distribution, for example, can result in different horizontal U_s for data sets of different spatial resolutions. Figure 4b shows a heterogeneous load distribution and the resulting deformation at 10 fictive GNSS stations computed using

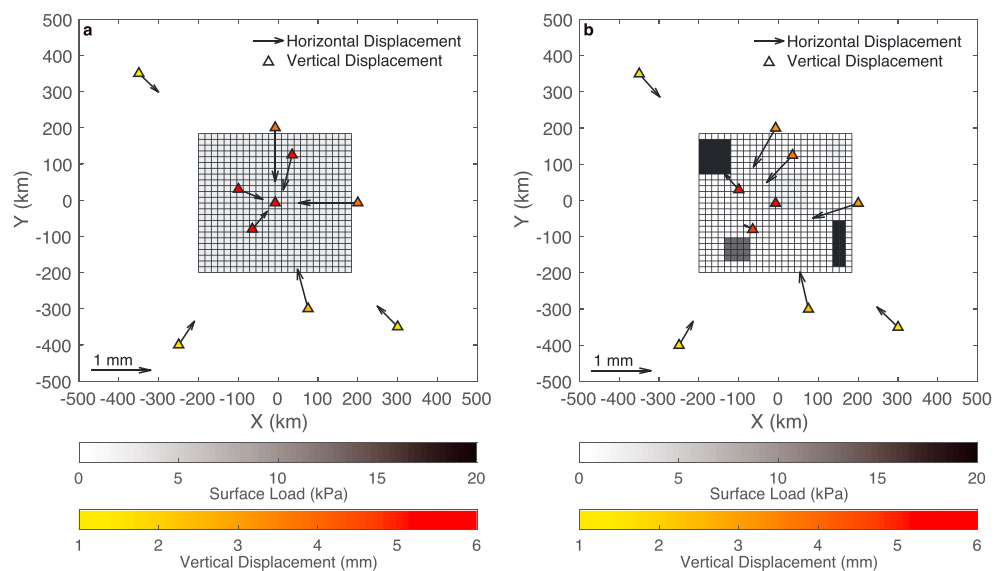


Figure 4. Deformation induced by (a) homogeneous and (b) heterogeneous load distribution (grey scale), measured at 10 fictive GNSS stations (triangles). Scenarios (a) and (b) are representative of the spatial resolution of GRACE and GNSS measurements, respectively.

Table 2
Mean Absolute Errors (MAE) Between GNSS Data and Different vbICA Reconstructions

vbICA reconstruction	Degrees >1			All degrees		
	East	North	Vertical	East	North	Vertical
	Arabian Peninsula					
Combined	18.89	12.44	55.80	22.99	16.13	52.98
Horizontal/Vertical	18.28	12.53	54.82	21.01	17.93	53.38
	Nepal Himalaya					
Combined	34.38	31.87	115.70	31.66	34.70	112.99
Horizontal/Vertical	35.66	32.73	115.73	32.76	35.49	113.93

a simple Boussinesq forward model (Boussinesq, 1885). In Figure 4a, the same total load is instead averaged out over the entire 400×400 km area to simulate the resolution of the GRACE data set. Calculating the deformation induced at these same 10 stations, we find that the horizontal displacements are different than in (b), even though these two scenarios present the same total load. Discrepancies in displacements are observed in the horizontal direction, but the vertical distributions display a similar pattern independent of load heterogeneity. This is consistent with what we observe in real GNSS data sets. Note that discrepancies only arise for the stations inside the loaded area; stations outside the loaded patch feel a similar effective load whether the distribution is averaged out or not.

Modeling these local effects goes beyond the goals of this paper and requires a more refined surface load distribution that can be achieved through integrated models relying on local meteorological data for example. Ultimately, since we use the U s from the GNSS data set to reconstruct the desired signal from the seasonal V s, such local effects are inherently modeled by the technique. Thus, our conclusions regarding the origin of the seasonal geodetic signal remain unchanged in light of these diverging U s.

As for the second IC, the correlation between V_2^{GNSS} and V_2^{GRACE} ($\rho = 0.164$; Table 1; Figure 3d) does not satisfy the criterion in Step (4c). The quasi-perpendicularity of the directions of the horizontal responses of U_2^{GNSS} and U_2^{GRACE} reinforces the idea that the two signals are not related; that is, IC_2^{GNSS} cannot be attributed to surface load variations. Considering the power spectral density (PSD) distribution of the temporal functions in Figure 3e, V_2^{GNSS} displays a mix of quasi-annual and quasi-biannual signals, whereas V_2^{GRACE} shows annual and multiannual signals (Figure 3e). Given that the PSD of V_2^{GNSS} peaks around the first and second draconitic harmonics, we instead attribute IC_2^{GNSS} to draconitic effects known to affect GNSS measurements (Ray et al., 2008). Draconitic effects are systematic errors in geodetic products most likely due to orbit modeling deficiencies. The resulting signals being spatially correlated, with a spatial correlation a priori distinct from the loading processes, we expect vbICA to be able to discriminate them from true deformation signals. Figure S2 shows that V_2^{GNSS} can indeed be explained by a sum of sinusoids with periods corresponding to the first 6 draconitic harmonics (351.6, 175.8, 87.9, 44.0, 22.0, and 11.0 days). Mean absolute errors (MAE) between the GNSS data set and the vbICA time series reconstructed with the seasonal IC_1^{GNSS} , and the draconitic IC_2^{GNSS} are listed in Table 2. MAE values are considerably higher in the vertical because the signal is stronger in this direction.

3.2. Nepal Himalaya

The Nepal Himalaya represents a more intricate case due to its more complex hydrological loading pattern. The procedure once again prescribes a two components vbICA as presented in Figure 5. In this case, the temporal functions from both data sets are all seasonal and the correlation coefficients are highest for the pairs $V_1^{\text{GNSS}} - V_1^{\text{GRACE}}$ ($\rho = 0.825$; Table 1 and Figure 5a) and $V_2^{\text{GNSS}} - V_2^{\text{GRACE}}$ ($\rho = 0.628$; Table 1 and Figure 5d). We thus argue that both IC_1^{GNSS} and IC_2^{GNSS} should be related to hydrological processes. The vertical patterns of U_1^{GNSS} and U_1^{GRACE} are in good agreement, while the horizontal distribution of U_1^{GNSS} is again quite heterogeneous compared to U_1^{GRACE} . Considering U_2^{GNSS} and U_2^{GRACE} , we notice a substantial improvement and degradation in the agreement of the horizontal and vertical patterns, respectively. In light of these observations, it is useful to consider the nature of the load by considering the gravimetric data presented in section 2.1.2. Movie S1 in the supporting information shows a migration of the load distribution over time, from southeast to central Asia. This trend corresponds to the Indian Monsoon regime, which causes heavy precipitations during the summer months (Bettinelli et al., 2008). This load pattern cannot be considered stationary as the Monsoon first hits the eastern Himalaya and gradually sweeps westward over the whole arc during the summer. This process results in a westward moving source of load. Since vbICA assumes nonmoving sources (section 2.2), multiple components are necessary to fully recover the effects of the propagating Monsoon load. For the special case of a source moving at a constant speed in a constant direction, we find that two components are sufficient to explain the observations and that these two components must be derivatives of one another. Text S1 presents an analytical proof of these results valid

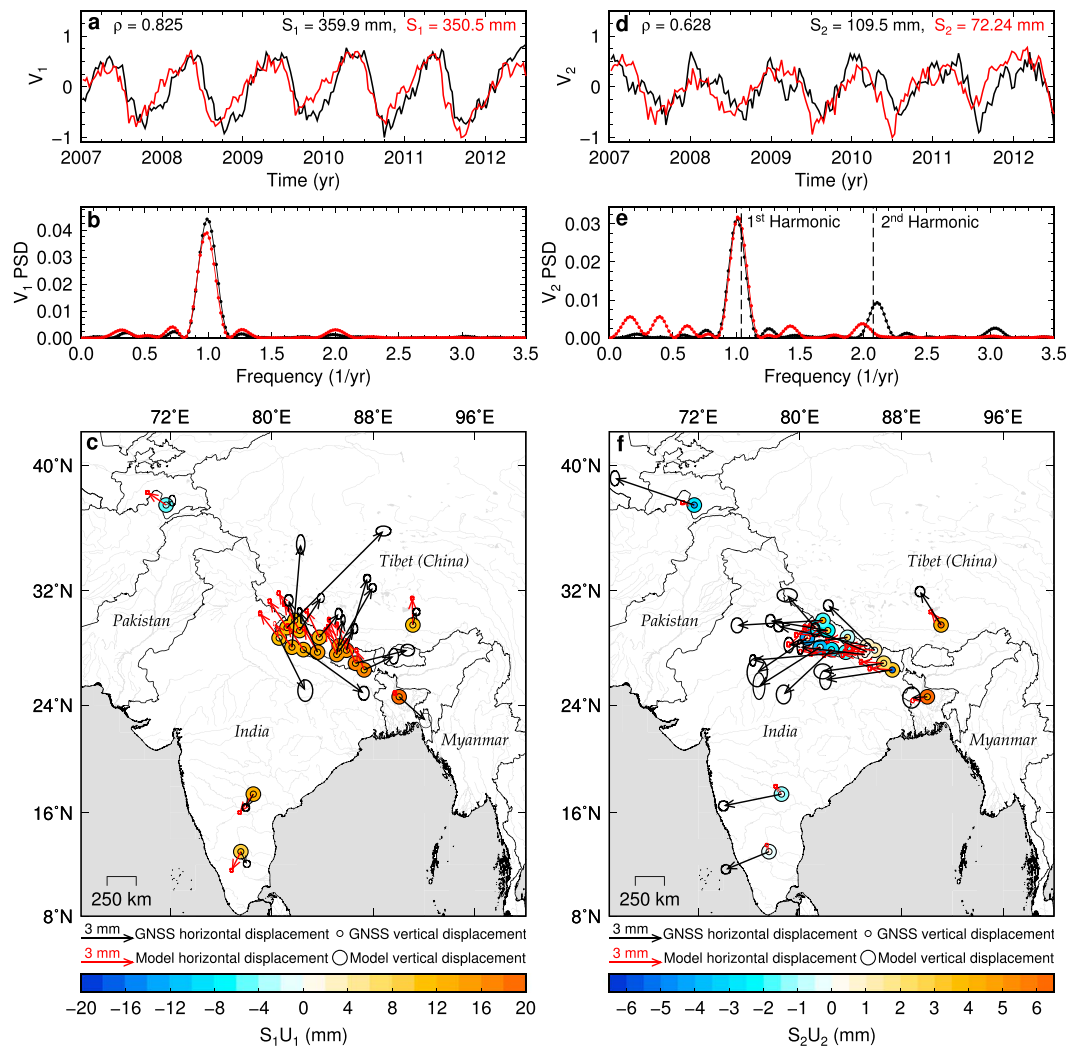


Figure 5. Same as Figure 3 but for the Himalayan case. In this case, both pairs of ICs are seasonal and matching.

for simple harmonic loads and the Boussinesq forward model in Figure 6 demonstrates that these findings might hold for a broader category of deformation fields (i.e., the temporal functions do not need to be simple sinusoids and the spatial mixing factors do not need to be harmonic). In Figure 6, we first compute the deformation induced by a load propagating to the right with the temporal function shown in Figure 6a. After performing a vbICA on the resulting deformation field, we find that two components are indeed sufficient to explain all of the data variance and that the second component is the derivative of the first component as indicated by the excellent fit between the black and red lines in Figure 6d. Moreover, IC_1 is associated with the loading pattern itself, whereas IC_2 is related to the motion of the loading pattern, which is consistent with what we observe in the Nepal Himalaya. Since in the Himalaya we indeed find that V_2^{GNSS} approximates the derivative of V_1^{GNSS} (Figure S3), we conclude that the two ICs are likely expressing the moving nature of the Monsoonal load. The fact that the horizontal patterns of U_2^{GNSS} and U_2^{GRACE} both point in the direction of load migration further supports this conclusion. Discrepancies in amplitudes between the two data sets (e.g., $S_2^{GNSS} > S_2^{GRACE}$) could be due to thermal, poroelastic, and atmospheric effects not captured by the GRACE satellites (Dong et al., 2002).

As for draconitic effects in the Nepal Himalaya, there is a quasi-biannual signal present in V_2^{GNSS} , which approximately corresponds to the second draconitic harmonic, meaning that the draconitic effect might have infiltrated IC_2^{GNSS} . A decomposition with three ICs (Figure S4) still shows the same features for the first

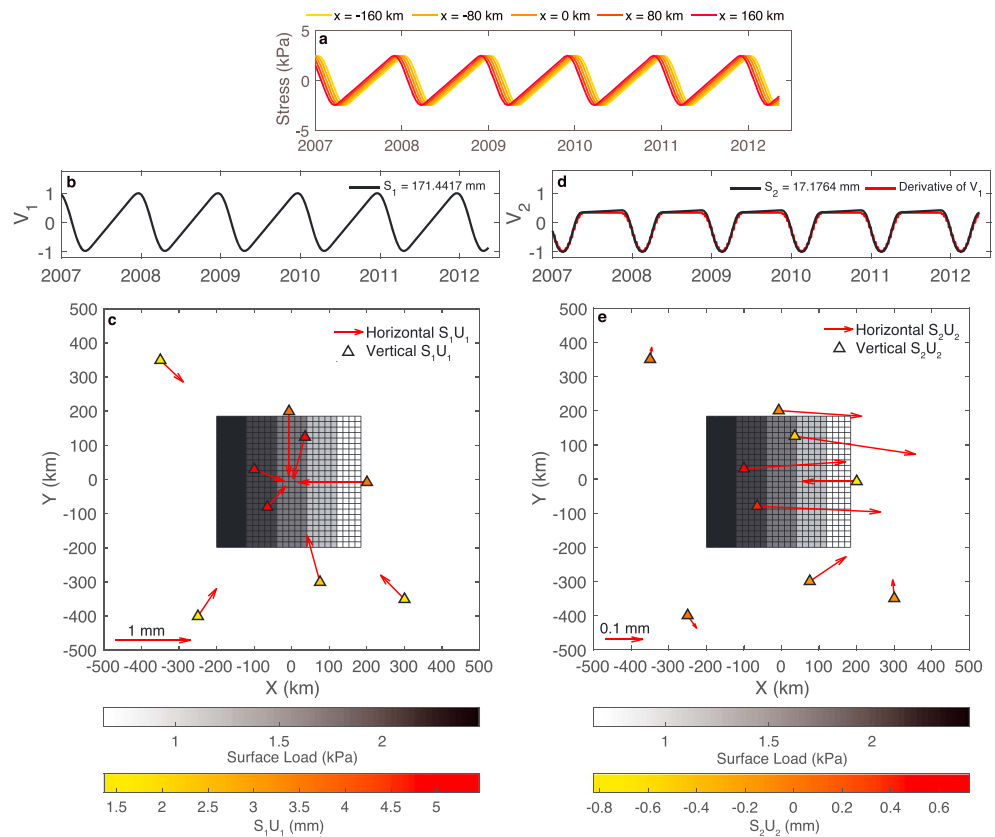


Figure 6. Two-component variational Bayesian Independent Component Analysis (vbICA) decomposition of a load pattern moving to the right at a constant velocity with a nonsymmetric temporal function. (a) Temporal load evolution at different point along the loaded patch. (b and d) Temporal functions corresponding to IC₁ and IC₂. The red curve in (d) corresponds to the derivative of IC₁. (c and e) Load distribution (in shades of grey) and vbICA spatial distribution (in yellow to red colors).

two ICs, but V_3^{GNSS} and V_3^{GRACE} do not display an acceptable correlation ($\rho = 0.346$; Figure S4g), indicating that IC₃^{GNSS} is likely not related to surface loading. An analysis of the associated PSD (Figure S4h) reveals that V_3^{GNSS} peaks around the second draconitic harmonic but not around the first. Given that S_2^{GNSS} is considerably higher than S_2^{GRACE} , it is possible that part of the annual signal in IC₂^{GNSS} is due to first harmonic draconitic effects. Draconitic errors usually exhibit a long-wavelength spatial pattern. Thus, one reason why the first draconitic harmonic signal may be absorbed into the annual component in Himalaya but not in Arabia is because the hydrological signal is of longer wavelength in Himalaya. Moreover, looking at the sum of sinusoids fit of V_2^{GNSS} in Figure S5, we see that in addition to the annual and biannual periods, the first two draconitic harmonics play the most important role in reconstructing the signal. V_3^{GNSS} in Figure S6, on the other hand, can be mostly explained by the first two draconitic harmonics alone. We conclude that IC₃^{GNSS} is probably mostly draconitic and that there might be some leakage of IC₃^{GNSS} into IC₂^{GNSS}. MAE values from the vbICA reconstruction with IC₁^{GNSS} and IC₂^{GNSS} are presented in Table 2.

4. Variations to the General Procedure

4.1. Inclusion of the Degree-1 Contribution

Although we have previously removed the degree-1 contribution from the GNSS time series for comparison purposes, the degree-1 spherical harmonic deformation is important to consider since a significant portion of it is due to redistributions in very long wavelength hydrological mass. Identifying the origin of the degree-1 deformation field as recorded by GNSS stations has major implications for reference frame definitions.

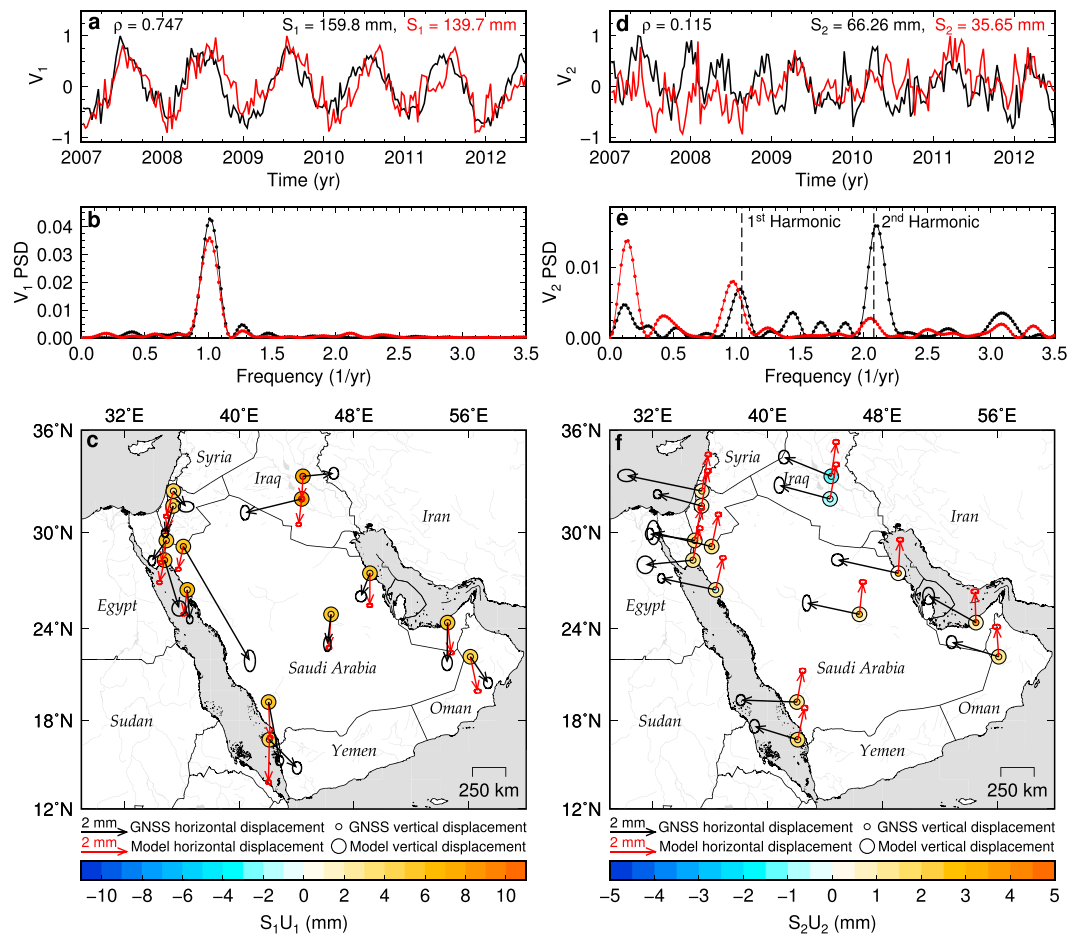


Figure 7. Same as Figure 3 but for the all-degrees case.

If the extracted seasonal signal is meant for hydrological studies, it would be preferable to perform the analysis directly on the original GNSS time series (i.e., not corrected for degree-1) and on the GRACE-derived time series to which the degree-1 contribution has been added as described in Chanard, Fleitout, Calais, Rebeschung, and Avouac (2018). The results from such analyses are presented in Figures 7 and 8 (and Figure S7) and the correlation coefficients and MAEs in Tables 1 and 2, respectively.

Unsurprisingly, the correlation coefficients for the $IC_{1,5}$ are larger for the all-degrees case than the degrees >1 analysis for both the Arabian Peninsula and the Nepal Himalaya. This is to be expected since a portion of the vbICA input, namely, the degree-1 contribution, is correlated in both data sets. The spatial correlations between the matching U^{GNSS} and U^{GRACE} are also better, especially in the Arabian Peninsula where the degree-1 contribution is a comparatively more important part of the seasonal signal. Although the correlation between U_2^{GNSS} and U_2^{GRACE} in the Himalaya is noticeably improved for the all-degrees case, the correlation coefficient between V_2^{GNSS} and V_2^{GRACE} is actually smaller in that case. We hypothesize that this may be due to the relative stationarity of the degree-1 deformation field compared to that of higher degrees, diminishing the importance of the propagation signal and thus making it harder to resolve by the vbICA. Nonetheless, given that the correlation coefficient is above the threshold of 0.50 and V_2^{GNSS} and V_2^{GRACE} are visibly matching, we still conclude that IC_1^{GNSS} and IC_2^{GNSS} for the Himalaya are most likely of hydrological origin.

Since we reach the same conclusions whether we apply the procedure to the data sets with or without the degree-1 contribution, we recommend doing the analysis without correcting the GNSS time series for the degree-1 deformation. This way, the resulting vbICA reconstruction will not depend on the choice of degree-1 field and will be readily useable for hydrological studies. Going through the procedure without

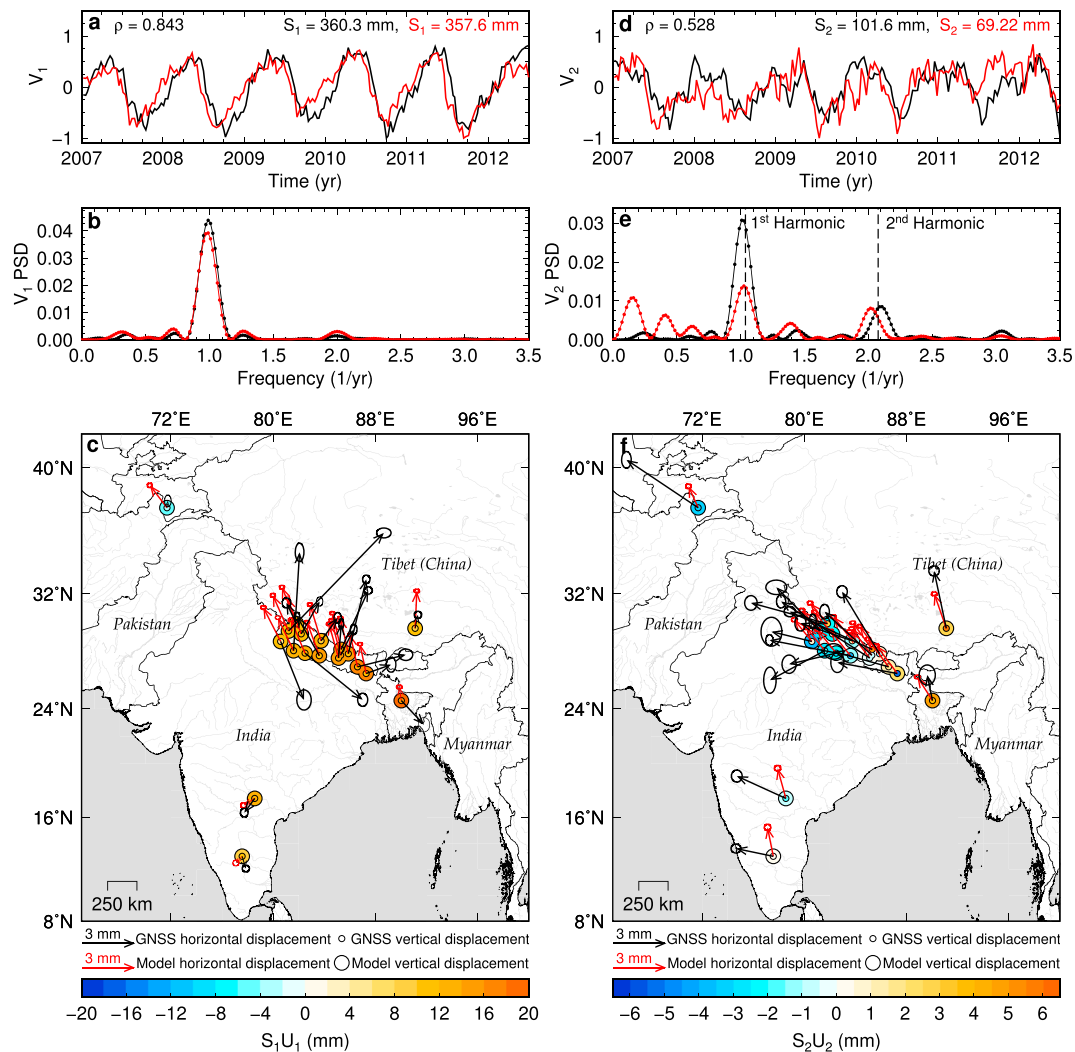


Figure 8. Same as Figure 5 but for the all-degrees case. See Figure S7 in the supporting information for a close-up view on Nepal.

the degree-1 contribution was still necessary, however, to demonstrate that the correlation between the IC_1^{GNSS} and IC_1^{GRACE} is not solely due to the GNSS-derived degree-1 contribution added to the GRACE data set. For reference, Figures S2, S3, and S5 are also presented for the all-degrees analysis to show that the discussion from section 3 still holds in this case.

4.2. Analysis on the Vertical and Horizontal Time Series Separately

Up to this point we have applied the procedure to the vertical and horizontal time series simultaneously without questioning the validity of this combined approach. The intuitive reasoning behind this approach is that the vertical and horizontal deformation fields should have the same source. To evaluate the validity of our combined approach, we compare our results so far to that obtained through vbICAs performed separately on the vertical and horizontal time series (with degree-1; Figures 9 and 10). In both Arabia and Himalaya, we find that the IC_1^{GNSS} and IC_1^{GRACE} from the vertical decomposition are quite similar to those from the combined analysis. This is expected because vertical seasonal deformation is the dominant signal in these time series. For the horizontal analysis in Arabia, the decomposition does not seem to be separating the seasonal loading from the draconitic effects in the GNSS data set, thus resulting in a lower correlation coefficient between V_1^{GNSS} and V_1^{GRACE} . The horizontal decomposition also does not perform as well in Nepal as V_2^{GRACE} does not match V_2^{GNSS} , possibly because the horizontal direction is largely affected by localized loads in the mid/high range (e.g., rivers) that GRACE averages out. This effect is smoothed out

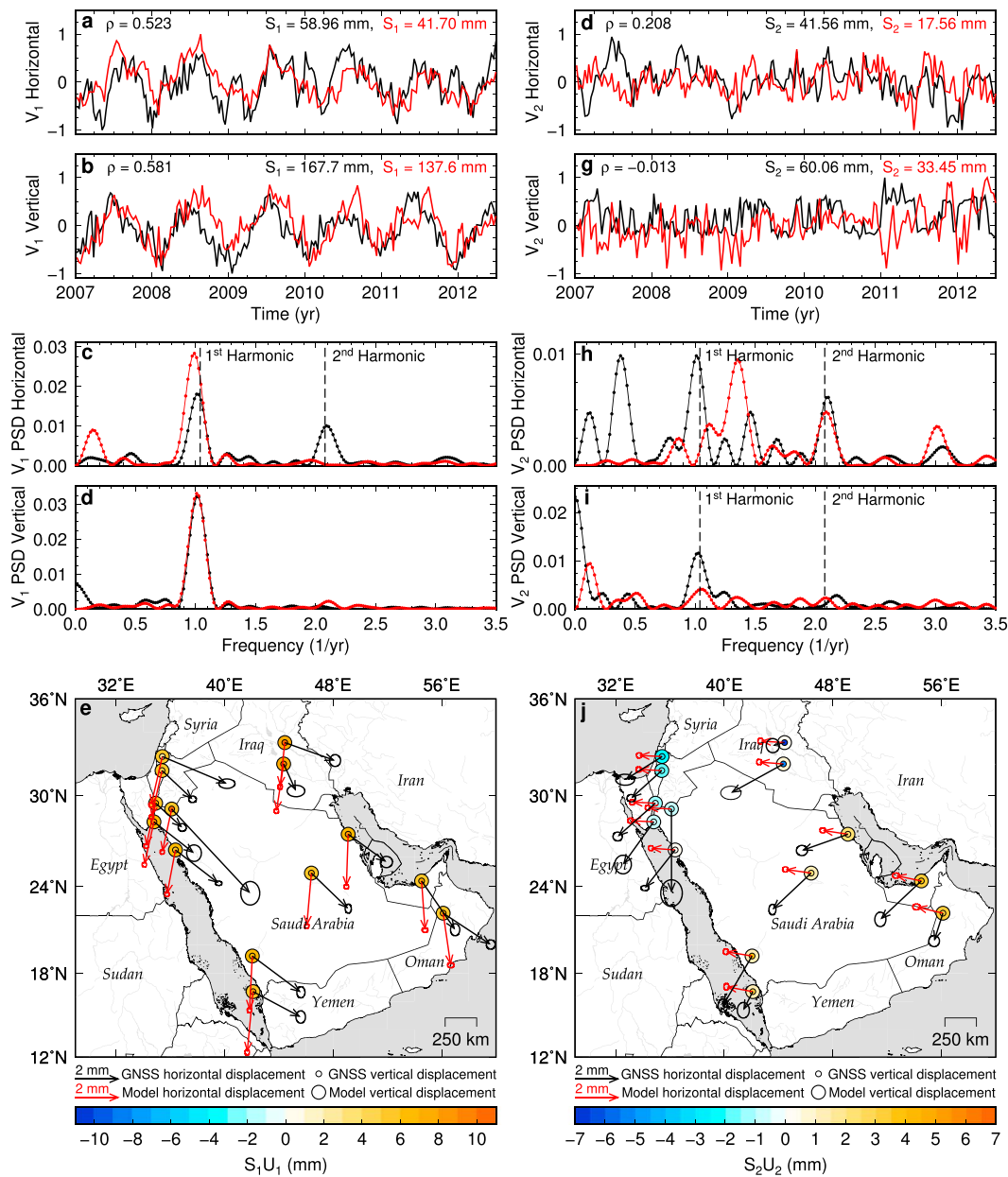


Figure 9. Same as Figure 3 but for the vertical/horizontal, all-degrees analysis.

in the combined approach because the vertical direction is much less affected by small scale loads and therefore consistent with GRACE.

In terms of MAEs (Table 2), in the Himalaya, all values are smaller for the combined analyses than for the horizontal/vertical analyses. In the Arabian Peninsula, only about half the values are smaller for the combined analyses. However, looking at the sample GNSS time series and vbICA reconstructions from a combined and a vertical/horizontal analysis in Figure S8, the fit to the east and north directions is visually better for the combined case. This is because the separated analysis does a poor job at capturing the weak but still existent seasonal signal in the east and north time series. We hypothesize that this is because the signal is too weak to be captured by the vbICA in the horizontal time series alone. Thus, unless the approach in which the horizontals and verticals are separated is improved, we advocate for the combined approach.

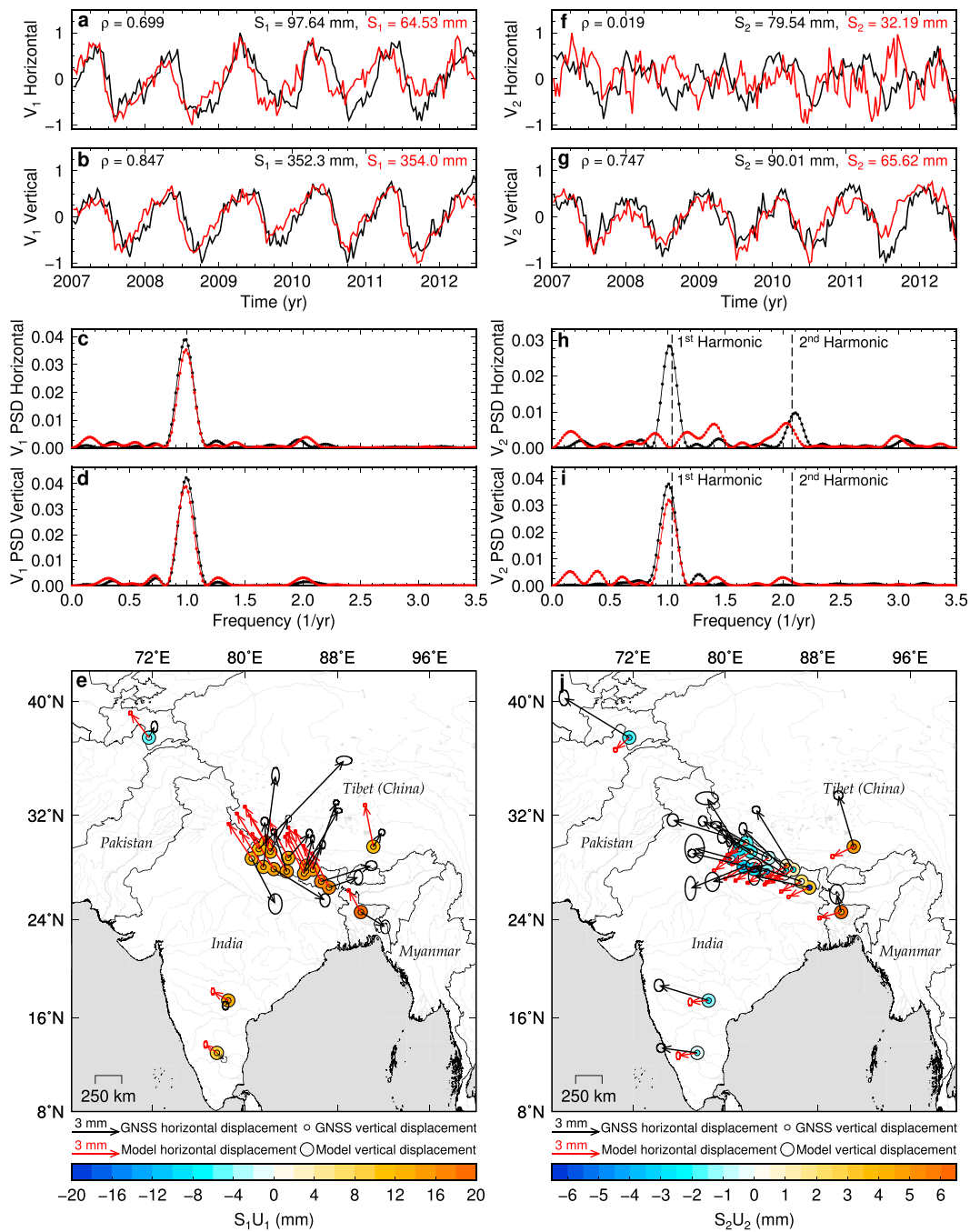


Figure 10. Same as Figure 5 but for the vertical/horizontal, all-degrees analysis.

5. Discussions and Conclusions

We have shown that supplementing a GRACE-based deformation model with a vbICA provides an efficient and accurate means of isolating surface load contributions from geodetic time series. We used the fact that GNSS and GRACE-derived displacements yield consistent time functions in both the Arabian Peninsula and the Nepal Himalaya to validate the origin of the ICs^{GNSS} related to continental water mass variations. Specifically, we recommend following the proposed procedure presented in section 2.3 with the vbICA performed simultaneously on the horizontal and vertical time series including the degree-1 deformation field (as presented in Figures 7 and 8) since, of the different analyses presented in this work, it is the

simplest and most robust approach to recover the complete surface load variation signal from the GNSS time series.

To correct the GNSS data set for these seasonal effects, we suggest to directly subtract the matched ICs^{GNSS} from the geodetic time series as opposed to subtracting the associated ICs^{GRACE}. We argue that this approach is more accurate in filtering out the nontectonic seasonal signals than the latter as GNSS stations are sensitive to local effects that are smoothed out by the GRACE data acquisition and processing. Figure S1 shows examples of vbICA reconstructions and corrected GNSS time series using this approach. MAE values are also presented in map format in Figures S9 and S10. Moreover, once an IC^{GNSS} in a given region has been identified as being caused by surface load variations by comparison with the GRACE-derived data set over a sufficiently long timespan, redoing the comparison would not be strictly necessary if a similar IC^{GNSS} is obtained from a vbICA in the same region but over a longer time span. In other words, the method could still be useful for epochs with missing GRACE data.

Although both study areas display a single hydrological seasonal source, we retain two ICs to correct the GNSS time series to account for (1) draconitic errors in the case of Arabia and (2) the migratory behavior of the load in Nepal. In the latter case, a third IC is related to the GNSS draconitic error, here considered as noise. Since the SNR between the hydrological signal and the draconitic error is larger in Nepal than Arabia, it is reasonable to expect this noise to appear in higher components, although not strictly necessary to reproduce the observations to first order as seen in Figure 2c. Nonetheless, the fact that vbICA is able to discriminate at least part of the draconitic error from the hydrological signal for the low SNR scenario is a major strength of the proposed procedure. Moreover, we recognize that the decision to retain only two components for the decompositions is influenced by our choice of a priori hyper-parameters in the vbICA. Even if ICA is not meant to decompose the data set in terms of variance maximization, an alternative approach could be to select the number of components by setting a minimum threshold on the amount of variance explained. In either case, selecting the number of components remains a case-dependent decision in which expert judgment still plays an important role.

The two complementary examples shown in this work demonstrate that the procedure is robust to complexities associated with spatial heterogeneities (e.g., local mass anomaly, poroelastic and thermoelastic deformation and regional deviation from preliminary reference Earth model) and simple moving loads. The technique can also help to isolate systematic errors in geodetic products, especially in low SNR ratio scenarios as is the case in Arabia. In a tectonically active region like Nepal, the technique can be used to investigate the link between seasonal loading and seismic activity.

It should be noted that although the technique aims to identify components that share the same physical mechanism across the two data sets, what the procedure is actually doing is identifying GNSS components that follow the same temporal pattern as surface load variations measured with GRACE. If there happened to be a source of deformation different but in phase with the GRACE components, then the seasonal signal extracted from the GNSS data might not be entirely caused by surface loading. A prime candidate for this is thermoelastic deformation of solid Earth (Ben-Zion & Leary, 1986; Fang et al., 2014; Tsai, 2011) and /or eventually of the GNSS monuments (Yan et al., 2009). Since, in the two study areas presented here, the temporal pattern and the amplitude of the GNSS seasonal signal agree fairly well with the prediction made from GRACE, we are confident that thermoelastic deformation is not a dominant effect in these regions. It could however be more significant in other regions, and the geodetic signal could then represent the combined effect of surface load and surface temperature variations if both signals were in phase.

Now that this methodology has been benchmarked for seasonal signals, a similar technique could be developed to capture multiannual hydrological trends, which could provide new insights into Earth's rheology (Chanard, Fleitout, Calais, Barbot, & Avouac, 2018). When additional ICs are included in the analysis, the technique can also be used to compare them with nonhydrological sources of known temporal behavior to help validate their physical causes. In fact, any data set with a spatio-temporal structure can be analyzed with the vbICA algorithm, making the approach suitable for the study of other geophysical problems. For example, a similar procedure could be applied to seismological data to study the effects of hydrology on seismic velocities. The kind of techniques describe in this study will also be particularly useful in exploiting the upcoming data set from the GRACE Follow-On mission, which will benefit from better procedures to relate surface hydrology and transient geodetic strain.

Acknowledgments

This study was partially supported by NSF award EAR-1821853 to J. P. A. and the King Abdullah City for Science and Technology. This work has greatly benefited from GNSS and GRACE data processed by NGL (<http://geodesy.unr.edu>; Blewitt et al., 2018) and CNES/CRGS (<http://grgs.obs-mip.fr>), respectively. We thank two anonymous reviewers for their detailed and constructive comments, which have led to an improved and more thorough manuscript. We also thank Don Argus and Victor Tsai for fruitful discussions.

References

- Argus, D. F., Fu, Y., & Landerer, F. W. (2014). Seasonal variation in total water storage in California inferred from GPS observations of vertical land motion. *Geophysical Research Letters*, *41*, 1971–1980. <https://doi.org/10.1002/2014GL059570>
- Bassin, C., Laske, G., & Masters, G. (2000). The current limits of resolution for surface wave tomography in North America. *Eos, Transactions of the American Geophysical Union*, *81*, F897.
- Ben-Zion, Y., & Leary, P. (1986). Thermoelastic strain in a half-space covered by unconsolidated material. *Bulletin of the Seismological Society of America*, *76*, 1447–1460.
- Bettinelli, P., Avouac, J. P., Flouzat, M., Bollinger, L., Ramillien, G., Rajaure, S., & Sapkota, S. (2008). Seasonal variations of seismicity and geotectonic strain in the Himalaya induced by surface hydrology. *Earth and Planetary Science Letters*, *266*(3–4), 332–344. <https://doi.org/10.1016/j.epsl.2007.11.021>
- Blewitt, G., Hammond, W. C., & Kreemer, C. (2018). Harnessing the GPS data explosion for interdisciplinary science. *Eos*, *99*. <https://doi.org/10.1029/2018EO104623>
- Blewitt, G., Lavallée, D., Clarke, P., & Nurutdinov, K. (2001). A new global mode of Earth deformation: Seasonal cycle detected. *Science*, *294*(5550), 2342–2345. <https://doi.org/10.1126/science.1065328>
- Bollinger, L., Perrier, F., Avouac, J. P., Sapkota, S., Gautam, U., & Tiwari, D. R. (2007). Seasonal modulation of seismicity in the Himalaya of Nepal. *Geophysical Research Letters*, *34*, L08304. <https://doi.org/10.1029/2006GL029192>
- Borsa, A. A., Agnew, D. C., & Cayan, D. R. (2014). Ongoing drought-induced uplift in the western United States. *Science*, *345*(6204), 1587–1590. <https://doi.org/10.1126/science.1260279>
- Boussinesq, J. (1885). *Application des potentiels à l'étude de l'équilibre et du mouvement des solides élastiques* (p. 1969). Blanchard: Reprint Paris.
- Bruinsma, S., Lemoine, J.-M., Biancale, R., & Valès, N. (2010). CNES/GRGS 10-day gravity field models (release 2) and their evaluation. *Advances in Space Research*, *45*(4), 587–601. <https://doi.org/10.1016/j.asr.2009.10.012>
- Cardoso, J. F., & Souloumiac, A. (1993). Blind beamforming for non-Gaussian signals. *IEE Proceedings F - Radar and Signal Processing*, *140*(6), 362–370. <https://doi.org/10.1049/ip-f-2.1993.0054>
- Carrère, L., & Lyard, F. (2003). Modeling the barotropic response of the global ocean to atmospheric wind and pressure forcing—Comparisons with observations. *Geophysical Research Letters*, *30*(6), 1275. <https://doi.org/10.1029/2002GL016473>
- Chan, K., Lee, T.-W., & Sejnowski, T. J. (2003). Variational Bayesian learning of ICA with missing data. *Neural Computation*, *15*(8), 1991–2011. <https://doi.org/10.1162/08997660360675116>
- Chanard, K., Avouac, J. P., Ramillien, G., & Genrich, J. (2014). Modeling deformation induced by seasonal variations of continental water in the Himalaya region: Sensitivity to Earth elastic structure. *Journal of Geophysical Research: Solid Earth*, *119*, 5097–5113. <https://doi.org/10.1002/2013JB010451>
- Chanard, K., Fleitout, L., Calais, E., Barbot, S., & Avouac, J.-P. (2018). Constraints on transient viscoelastic rheology of the asthenosphere from seasonal deformation. *Geophysical Research Letters*, *45*, 2328–2338. <https://doi.org/10.1002/2017GL076451>
- Chanard, K., Fleitout, L., Calais, E., Rebeschung, P., & Avouac, J.-P. (2018). Toward a global horizontal and vertical elastic load deformation model derived from GRACE and GNSS station position time series. *Journal of Geophysical Research: Solid Earth*, *123*, 3225–3237. <https://doi.org/10.1002/2017JB015245>
- Comon, P. (1994). Independent component analysis, a new concept? *Signal Processing*, *36*(3), 287–314. [https://doi.org/10.1016/0165-1684\(94\)90029-9](https://doi.org/10.1016/0165-1684(94)90029-9)
- Craig, T. J., Chanard, K., & Calais, E. (2017). Hydrologically-driven crustal stresses and seismicity in the New Madrid Seismic Zone. *Nature Communications*, *8*(1), 2143. <https://doi.org/10.1038/s41467-017-01696-w>
- Davis, J. L., Elósegui, P., Mitrovica, J. X., & Tamisiea, M. E. (2004). Climate-driven deformation of the solid Earth from GRACE and GPS. *Geophysical Research Letters*, *31*, L24605. <https://doi.org/10.1029/2004GL021435>
- Dong, D., Fang, P., Bock, Y., Cheng, M. K., & Miyazaki, S. (2002). Anatomy of apparent seasonal variations from GPS-derived site position time series. *Journal of Geophysical Research*, *107*(B4), 2075. <https://doi.org/10.1029/2001JB000573>
- Dong, D., Yunck, T., & Hefflin, M. (2003). Origin of the international terrestrial reference frame. *Journal of Geophysical Research*, *108*(B4), 2200. <https://doi.org/10.1029/2002JB002035>
- Drouin, V., Heki, K., Sigmundsson, F., Hreinsdóttir, S., & Ófeigsson, B. G. (2016). Constraints on seasonal load variations and regional rigidity from continuous GPS measurements in Iceland, 1997–2014. *Geophysical Journal International*, *205*(3), 1843–1858. <https://doi.org/10.1093/gji/ggw122>
- Dziewonski, A. M., & Anderson, D. L. (1981). Preliminary reference Earth model. *Physics of the Earth and Planetary Interiors*, *25*(4), 297–356. [https://doi.org/10.1016/0031-9201\(81\)90046-7](https://doi.org/10.1016/0031-9201(81)90046-7)
- Fang, M., Dong, D. N., & Hager, B. H. (2014). Displacements due to surface temperature variation on a uniform elastic sphere with its centre of mass stationary. *Geophysical Journal International*, *196*(1), 194–203. <https://doi.org/10.1093/gji/ggt335>
- Farrell, W. E. (1972). Deformation of the Earth by surface loads. *Reviews of Geophysics and Space Physics*, *10*(3), 761–797. <https://doi.org/10.1029/RG010i003p00761>
- Fu, Y., Argus, D. F., & Landerer, F. W. (2015). GPS as an independent measurement to estimate terrestrial water storage variations in Washington and Oregon. *Journal of Geophysical Research: Solid Earth*, *120*, 552–566. <https://doi.org/10.1002/2014JB011415>
- Fu, Y., Freymueller, J. T., & Jensen, T. (2012). Seasonal hydrological loading in southern Alaska observed by GPS and GRACE. *Geophysical Research Letters*, *39*, L15310. <https://doi.org/10.1029/2012GL052453>
- Fu, Y. N., & Freymueller, J. T. (2012). Seasonal and long-term vertical deformation in the Nepal Himalaya constrained by GPS and GRACE measurements. *Journal of Geophysical Research*, *117*, B03407. <https://doi.org/10.1029/2011JB008925>
- Gualandi, A., Avouac, J. P., Galetzka, J., Genrich, J. F., Blewitt, G., Adhikari, L. B., et al. (2017). Pre- and post-seismic deformation related to the 2015, M(w)7.8 Gorkha earthquake, Nepal. *Tectonophysics*, *714–715*, 90–106. <https://doi.org/10.1016/j.tecto.2016.06.014>
- Gualandi, A., Nichele, C., Serpelloni, E., Chiaraluce, L., Anderlini, L., Latorre, D., et al. (2017). Aseismic deformation associated with an earthquake swarm in the northern Apennines (Italy). *Geophysical Research Letters*, *44*, 7706–7714. <https://doi.org/10.1002/2017GL073687>
- Gualandi, A., Serpelloni, E., & Belardinelli, M. E. (2016). Blind source separation problem in GPS time series. *Journal of Geodesy*, *90*(4), 323–341. <https://doi.org/10.1007/s00190-015-0875-4>
- Hyvärinen, A., & Oja, E. (1997). A fast fixed-point algorithm for independent component analysis. *Neural Computation*, *9*(7), 1483–1492. <https://doi.org/10.1162/neco.1997.9.7.1483>
- Jean, J., Meyer, U., & Jäggi, A. (2015). *Combination of monthly gravity field solutions from different processing centers* (Vol. 17, p. 5879). Vienna, Austria: Presented at the EGU General Assembly.

- Johnson, C. W., Fu, Y. N., & Burgmann, R. (2017). Seasonal water storage, stress modulation, and California seismicity. *Science*, 356(6343), 1161–1164. <https://doi.org/10.1126/science.aak9547>
- Ramillien, G., Frappart, F., Cazenave, A., & Guntner, A. (2005). Time variations of land water storage from an inversion of 2 years of GRACE geoids. *Earth and Planetary Science Letters*, 235(1–2), 283–301. <https://doi.org/10.1016/j.epsl.2005.04.005>
- Ray, J., Altamimi, Z., Collilieux, X., & Dam, T. v. (2008). Anomalous harmonics in the spectra of GPS position estimates. *GPS Solutions*, 12(1), 55–64. <https://doi.org/10.1007/s10291-007-0067-7>
- Serpelloni, E., Pintori, F., Gualandi, A., Scoccimarro, E., Cavaliere, A., Anderlini, L., et al. (2018). Hydrologically-induced karst deformation: Insights from GPS measurements in the Adria-Eurasia plate boundary zone. *Journal of Geophysical Research: Solid Earth*, 123, 4413–4430. <https://doi.org/10.1002/2017JB015252>
- Smeed, D. A. (2004). Exchange through the Bab el Mandab. *Deep Sea Research Part II: Topical Studies in Oceanography*, 51(4–5), 455–474. <https://doi.org/10.1016/j.dsr2.2003.11.002>
- Swenson, S., Chambers, D., & Wahr, J. (2008). Estimating geocenter variations from a combination of GRACE and ocean model output. *Journal of Geophysical Research*, 113, B08410. <https://doi.org/10.1029/2007JB005338>
- Tsai, V. C. (2011). A model for seasonal changes in GPS positions and seismic wave speeds due to thermoelastic and hydrologic variations. *Journal of Geophysical Research*, 116, B04404. <https://doi.org/10.1029/2010JB008156>
- van Dam, T., Wahr, J., Milly, P. C. D., Shmakin, A. B., Blewitt, G., Lavallee, D., & Larson, K. M. (2001). Crustal displacements due to continental water loading. *Geophysical Research Letters*, 28(4), 651–654. <https://doi.org/10.1029/2000GL012120>
- Wahr, J., Smeed, D. A., Leuliette, E., & Swenson, S. (2014). Seasonal variability of the Red Sea, from satellite gravity, radar altimetry, and in situ observations. *Journal of Geophysical Research: Oceans*, 119, 5091–5104. <https://doi.org/10.1002/2014JC010161>
- Yan, H., Chen, W., Zhu, Y., Zhang, W., & Zhong, M. (2009). Contributions of thermal expansion of monuments and nearby bedrock to observed GPS height changes. *Geophysical Research Letters*, 36, L13301. <https://doi.org/10.1029/2009GL038152>